Rational Transfer Function Models for Biofilm Reactors

Torsten Wik and Claes Breitholtz
Control Engineering Laboratory, Chalmers University of Technology, S-412 96 Göteborg, Sweden

Design of controllers and optimization of plants using biofilm reactors often require dynamic models and efficient simulation methods. Standard model assumptions were used to derive nonrational transfer functions describing the fast dynamics of stirred-tank reactors with zero- or first-order reactions inside the biofilm. A method based on the location of the singularities was used to derive rational transfer functions that approximate nonrational ones. These transfer functions can be used in efficient simulation routines and in standard methods of controller design. The order of the transfer functions can be chosen in a natural way, and changes in physical parameters may directly be related to changes in the transfer functions. Further, the mass balances used and, hence, the transfer functions, are applicable to catalytic reactors with porous catalysts as well. By applying the methods to a nitrifying trickling filter, reactor parameters are estimated from residence-time distributions and low-order rational transfer functions are achieved. Simulated effluent dynamics, using these transfer functions, agree closely with measurements.

Introduction

A biofilm can be characterized as an organic matrix consisting of a complex community of bacteria, algae, fungi, and protozoa embedded in organic polymers. In fixed biofilm reactors the biofilm is attached to substrata that, generally, are impermeable. Substrates diffuse from the bulk liquid into the biofilm where the bacteria carry out the desired transformations of substrates. Depending on the type of biofilm reactor, the biofilm substrata may be carrier material or fixed packing media that can be either structured or random. Typical examples of fixed biofilm reactors are: biological fluidized beds, biofilters of different kinds, moving bed reactors, rotating biological contactors, and trickling filters. Reactors of this kind have attained increased attention, particularly in drinking water and wastewater treatment due to the ability to withhold bacterial populations having low growth rates, and new materials that give high specific capacities.

The dynamics of biofilm reactors can be divided into slow modes and fast modes. The fast dynamics are mainly caused by the reactor hydraulics and diffusive mass transfer in the biofilm, while the slow dynamics are caused by the growth and decay of the organisms in the biofilm. These dynamic modes are generally separated by several orders of magnitude, since it generally takes several days for the fauna to change while the fast transients settle in less than an hour. Thus, the slow transients can often be ignored when only the fast dynamics are studied (Kissel et al., 1984).

Most of the reported dynamic modeling and work on biofilm reactors have been focused on the slow biofilm dynamics, which have effects on the operation of the plants over longer periods of time (Andersson et al., 1994; Boller et al., 1997). However, there are several reasons to investigate, to model, and to analyze the fast dynamics also. First of all, in the daily operation of a plant using biofilm reactors the fast dynamics often have to be taken into consideration to optimize the operation, and to guarantee stable control systems. The fast dynamics also play an important role for the reactor efficiency when the substrate load varies quickly (Rittmann, 1985). Further, since physically-based models of the fast dynamics are in many ways simplifications of more complex models of the slow dynamics, important model parameters are the same (Kissel et al., 1984; Gujer and Wanner, 1990; Wik and Breitholtz, 1996). Hence, parameter identification from experimental data, using models of the fast dynamics,

Correspondence concerning this article should be addressed to T. Wik.

can be a way of acquiring information about the slow dynamics as well.

A continuously stirred biofilm reactor (CSBR) can be defined as an ideally stirred tank reactor, where the reactions take place in a biofilm attached to impermeable substrata. Models, based on physical principles and standard assumptions, are presented of the fast dynamics for such CSBRs with biofilm substrata that are planar, cylindrical or spherical, and where the reaction rate inside the biofilm is of zero or first order.

Fixed biofilm reactors and catalytic reactors with porous catalysts have an attractive analogy, pointed out by, for example, Atkinson and Daoud (1968), which follows from the physics of the diffusion and the reaction in biofilms and in catalysts. Under the assumptions used in the development of the models, the mass balances are the same for the CSBRs and continuously stirred catalytic reactors with porous catalyst particles (Aris, 1975). Hence, the methods developed for the biofilm reactors also apply to such catalytic reactors if the reaction in the catalyst can be assumed to be of zero or first order.

Nonrational first principle transfer functions describing the dynamics caused by changes in influent concentrations are derived for the presented models. It is shown that the singularities of these transfer functions are located on the negative real axis with a distance between them that increases with distance from zero. Based on this fact, a method is introduced to derive low-order rational transfer functions that approximate the nonrational ones. These approximations have several appealing properties:

- Efficient routines for simulations using the rational transfer function models are available in most types of numerical software.
- Many standard methods of controller design require rational transfer functions.
- The derivation only requires Newton-Raphson searches for the values of the singularities and evaluation of a few expressions.
- Changes in physical parameters, in particular the first-order rate coefficient that may depend significantly on temperature, can easily be related to changes in the transfer function.
- Since the approximation is based on truncation of a sum of first-order transfer functions with decreasing time constants and decreasing gain, the order of the approximate transfer function can be chosen for a specific application in a natural way and without any recalculations.

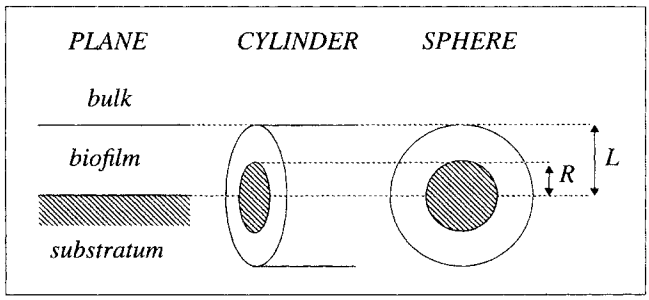

Figure 1. Biofilm and biofilm substrata.

The use of the transfer function models is illustrated by an application of the methods to a nitrifying trickling filter used for treating municipal tertiary wastewater. Using the transfer functions and data from residence time distribution tests carried out on the plant, biofilm and reactor parameters are estimated. With the estimated values, low-order rational transfer functions are derived for the plant. The dynamics of simulated effluent concentrations, using such a transfer function, agree with measurements from a period of varying influent ammonium concentration and flow. Such rational transfer functions would, for example, be attractive in the feedforward control strategy suggested by Wik (1997) for reducing the amount of ethanol added in the denitrification process stage that, generally, follows nitrifying trickling filters.

Modeling

We model a CSBR as a continuously stirred tank with bulk volume V through which there is a flow Q of bulk liquid. The influent concentration is c^b_{in} and the effluent concentration, which equals that in the CSBR, is c^b. The substrate diffuses without transfer resistance into a biofilm where the reactions take place. For the biofilm, the following assumptions are made: (1) The substrate concentration (c) in the biofilm is continuous in time ($\bar{t}$) and space ($\bar{\xi}$); (2) the void fraction (ϵ) in the biofilm, the substrate diffusion coefficient (D), and the thickness of the biofilm are constant; (3) the transport of substrates inside the biofilm obeys Fick's law of diffusion in one dimension.

With these assumptions, a dimensionless mass balance over the bulk gives

$$\tau \frac{d}{dt} c^b = c^b_{\text{in}} - c^b - \gamma \left. \frac{\partial c}{\partial \xi} \right|_{\xi = 1}, \tag{1}$$

where $\tau = VD/(QL^2\epsilon)$, $\gamma = AD/(QL)$, and space and time are scaled as $\xi = \bar{\xi}/L$ and $t = \lambda \bar{t}$, where $\lambda = D/(L^2\epsilon)$. Here, A is the total area of biofilm in the CSBR, and L denotes the value of $\bar{\xi}$ at the biofilm surface (see Figure 1).

The equations describing the substrate concentrations inside the biofilm depend on the shape of the substrata and on the reaction kinetics. Typically, the rate at which the bacteria carry out the transformations of substrates follows a nonlinear saturation function, such as a Monod expression in one of the involved substrates. If the concentration is above the saturation level, or if we are interested in modeling other substrates than the rate limiting one, the reaction rate will be of zero order. At low concentrations, the rate can be assumed to be first order with respect to the limiting substrate. In an intermediate region, the rate may often be linearized around an operating point. Here, we assume that the reaction rate is a linear function of the substrate concentration modeled. Three different shapes are considered: Planar, cylindrical and spherical (see Figure 1). The effects of the cylinder ends are ignored, that is, the cylinders are assumed long compared to their diameter. If the dimensionless zero-order rate coefficient is denoted μ, which may depend on ξ, and the first-order rate coefficient is denoted κ, the following equations hold for the different shapes of substrata

Planes

Mass balance

$$\frac{\partial c}{\partial t} = \frac{\partial^2 c}{\partial \xi^2} - \kappa c - \mu, \quad 0 < \xi < 1. \tag{2}$$

Boundary conditions

$$\frac{\partial c}{\partial \xi} = 0, \quad \xi = 0 \quad \text{and} \quad c = c^b, \quad \xi = 1.$$

Spheres and cylinders

Mass balance

$$\frac{\partial c}{\partial t} = \frac{p}{\xi}\frac{\partial c}{\partial \xi} + \frac{\partial^2 c}{\partial \xi^2} - \kappa c - \mu, \quad \rho < \xi < 1. \tag{3}$$

Boundary conditions

$$\frac{\partial c}{\partial \xi} = 0, \quad \xi = \rho \quad \text{and} \quad c = c^b, \quad \xi = 1,$$

where $p = 2$ for spheres, $p = 1$ for cylinders, and $\rho = R/L$ (see Figure 1). When $\rho = 0$, the inner boundary condition should be replaced by c being bounded at $\rho = 0$.

After subtraction of the stationary solutions ($\bar{c}$ and $\bar{c}^b$) and Laplace transformation of Eqs. 2 and 3, and the boundary conditions, the solutions $C = \mathcal{L}\{c - \bar{c}\}$ for each shape follow from the solutions of the corresponding stationary problems (Aris, 1975, pp. 136–137)

$$C(\xi, s) = \begin{cases} C^b(s)\dfrac{\cosh \xi z}{\cosh z} & \text{(plane)} \\ C^b(s)\dfrac{I_0(\xi z)K_1(\rho z) + K_0(\xi z)I_1(\rho z)}{I_0(z)K_1(\rho z) + K_0(z)I_1(\rho z)} & \text{(cylinder)} \\ C^b(s)\dfrac{1}{\xi}\dfrac{z\rho\cosh z(\xi - \rho) + \sinh z(\xi - \rho)}{z\rho\cosh z(1-\rho) + \sinh z(1-\rho)} & \text{(sphere)}, \end{cases}$$

where $z = \sqrt{s + \kappa}$, I_0 and I_1 are modified Bessel functions of the first kind, of zero and first order, and K_0 and K_1 are modified Bessel functions of the second kind, of zero and first order.

Laplace transformation of Eq. 1 and insertion of the derivatives of the above expressions for $C(\xi, s)$ at $\xi = 1$ give the following transfer function for a CSBR

$$G(s) = \frac{C^b(s)}{C^b_{\text{in}}(s)} = \frac{K}{1 + \tilde{\tau}z^2 + \tilde{\gamma}M(z)}, \tag{4}$$

where $K = 1/(1 - \tau\kappa)$, $\tilde{\tau} = K\tau$, $\tilde{\gamma} = K\gamma$. The function $M(z)$ depends on the shape of the substrata

$$M(z) = \begin{cases} z\tanh z & \text{(plane)} \\ z\dfrac{K_1(\rho z)I_1(z) - K_1(z)I_1(\rho z)}{K_1(\rho z)I_0(z) + K_0(z)I_1(\rho z)} & \text{(cylinder)} \\ -1 + z\dfrac{\rho z\sinh \delta z + \cosh \delta z}{\rho z\cosh \delta z + \sinh \delta z} & \text{(sphere)}, \end{cases}$$

where $\delta = 1 - \rho$ is the dimensionless biofilm thickness. Note that the zero-order rate coefficient μ has no effect on how changes in influent concentration affect the effluent concentration.

For biofilms on no substrata in the same shapes, that is, planar slabs of thickness $2L$, cylinder flocs ($\rho = 0$) and sphere flocs ($\rho = 0$), values for $M(z)$ remain the same for the slabs but simplify to $zI_1(z)/I_0(z)$ for cylinders and $-1 + z\coth z$ for spheres.

Transfer Function Singularities

For the presented method to derive rational transfer functions, the locations of the singularities of the transfer function $G(s)$ must be known. The singularities follow from setting the denominator in $G(s)$ equal to zero

$$1 + \tilde{\tau}z^2 + \tilde{\gamma}M(z) = 0, \tag{5}$$

or equivalently

$$M(z) = -\frac{\tau}{\gamma}\left(z^2 + \frac{1}{\tau} - \kappa\right). \tag{6}$$

In the Appendix it is shown that, if $z = x + iy$, the imaginary part of $M(z)$ has the same sign as xy for all shapes considered. Since the sign of the imaginary part of the righthand side equals that of $-xy$, all possible solutions to Eq. 6 must be located on the real and imaginary axes.

On the real axis, $M(x)$ is a positive even function for all shapes. Hence, solutions to Eq. 6 may exist on the real axis only if $\kappa > 1/\tau$ ($\tilde{\gamma}$ and $\tilde{\tau}$ less than zero). The solutions are centered around $x = 0$, where the positive solutions are less than $\sqrt{\kappa - 1/\tau}$. Hence, both the real solutions $z = x$ and the imaginary solutions $z = iy$ to Eq. 6 result in singularities to $G(s)$, that is, $\alpha = z^2 - \kappa$, located on the negative real axis. This implies that the CSBR-system is stable, that is, bounded changes in influent concentration can never cause uncontrolled oscillations in the effluent concentration from the reactor.

Since $M(x)$ is monotonous for $x > 0$, there may be only one negative singularity $\alpha = x^2 - \kappa$ corresponding to a real solution x to Eq. 6. Below, it will be shown that the remaining singularities $\alpha = -y^2 - \kappa$, corresponding to imaginary solutions iy to Eq. 6, are located in nonoverlapping intervals of increasing size. Because the singularities are then spread out along the negative real axis with larger and larger distances between them they are *countable*, a fact that will be used in the derivation of rational approximations of $G(s)$. Knowing the approximate locations of the singularities, they may readily be found numerically by a Newton-Raphson method, for example.

Planes

Using $\tanh iy = i \tan y$, the solutions to Eq. 6 on the imaginary axis are given by

$$\tilde{\gamma} \tan y = \frac{1}{y} - \tilde{\tau} y. \tag{7}$$

The solutions to this equation are centered around $y = 0$. When $\tilde{\tau}$ and $\tilde{\gamma}$ are positive, the positive solutions satisfy

$$0 < y_1 < \frac{\pi}{2} < y_2 < \frac{3\pi}{2} < y_3 < \frac{5\pi}{2} < y_4 < \ldots \tag{8}$$

and when $\tilde{\tau}$ and $\tilde{\gamma}$ are negative, the positive solutions satisfy

$$\frac{\pi}{2} < y_1 < \frac{3\pi}{2} < y_2 < \frac{5\pi}{2} < y_3 < \ldots,$$

Cylinders

Using the relations $I_n(iy) = i^n J_n(y)$, $K_n(iy) = (\pi/2) i^{n+1} [J_n(y) + iY_n(y)]$, where J_n and Y_n are Bessel functions of the first and second kind and of order n, it follows that the solutions $z = iy$ to Eq. 5 on the imaginary axis are given by

$$\tilde{\gamma} \frac{J_1(\rho y) Y_1(y) - Y_1(\rho y) J_1(y)}{Y_1(\rho y) J_0(y) - Y_0(y) J_1(\rho y)} = \frac{1}{y} - \tilde{\tau} y.$$

The expression on the lefthand side is the quotient of two equally damped oscillative functions of y. Hence, the solutions are restricted to the intervals between the zeros of the denominator. For large y the expression approaches $-\tilde{\gamma} \tan \delta y$, and then the singularities are located in intervals similar to those for planar coordinates.

When $\rho = 0$, the solutions are located between the zeros of J_0, which can be found in tables of Bessel functions (Råde and Westergren, 1990).

Spheres

On the imaginary axis, $M(z)$ becomes

$$M(iy) = \frac{\delta y - (1 + \rho y^2) \tan \delta y}{\rho y + \tan \delta y}$$

and Eq. 5 can be written

$$\tan \delta y = y \frac{\delta \tilde{\gamma} + \rho - \tilde{\tau} y^2}{\tilde{\gamma} - 1 + (\rho \tilde{\gamma} + \tilde{\tau}) y^2}.$$

As for planar coordinates, the solutions are constrained to the intervals between the singularities of $\tan \delta y$.

Rational Transfer Functions

The transfer function (Eq. 4) is not suitable for standard methods of simulation, optimization and controller design. Instead, rational functions for which there are numerous standard routines available in software, such as MATLAB and MATRIXx, are desired.

Rational approximations of $G(s)$ will be derived by first determining the exact unit impulse response (or weighting function), that is, the inverse Laplace transform of $G(s)$, and then finding a rational $\hat{G}(s)$ that arbitrarily well approximates the exact response. The theorems and definitions used can be found in standard textbooks on analytical functions (see, for example, Fischer, 1990).

Denote the denominator of $G(s)$ by $F(s)$. The inverse Laplace transform of $G(s)$ is then

$$g(t) = \lim_{\sigma \to \infty} \frac{1}{2\pi i} \int_{\kappa - i\sigma}^{\kappa + i\sigma} \frac{K e^{st}}{F(s)} ds.$$

Since the singularities are *countable* and located left of $s = \kappa$, we may use the Residue Theorem to determine the inverse Laplace transform

$$g(t) = \frac{1}{2\pi i} \oint_{\Omega} \frac{K e^{st}}{F(s)} ds \tag{9}$$

$$= K \sum_{k=1}^{\infty} \operatorname{Res} \left\{ \frac{e^{st}}{F(s)} \right\}_{s = \alpha_k}, \tag{10}$$

where α_k are the locations of the singularities of $G(s)$, and Ω is the region left of $s = \kappa$ in the complex plane.

The denominator $F(s)$ is analytic in a neighborhood of each singularity α_k of $G(s)$. Hence, there exists a convergent Taylor expansion around each singularity

$$F(s) = F(\alpha_k) + \left. \frac{dF}{ds} \right|_{s = \alpha_k} (s - \alpha_k) + \sum_{p=2}^{\infty} \frac{1}{p!} \left. \frac{d^p F}{ds^p} \right|_{s = \alpha_k} (s - \alpha_k)^p \tag{11}$$

where $F(\alpha_k) = 0$ and

$$F'(\alpha_k) = \left. \frac{dF}{ds} \right|_{s = \alpha_k} = \tilde{\tau} + \frac{\tilde{\gamma}}{2 z_k} \left. \frac{dM}{dz} \right|_{z = \sqrt{\alpha_k + \kappa}}.$$

Since the derivatives $F'(\alpha_k)$ are evaluated at intersection points between the rapidly changing left side of Eq. 6 and the square function on the right, $F'(\alpha_k)$ cannot be zero. Thus, the integrand in Eq. 9 has poles of order one at α_k and the residues are given by

$$\operatorname{Res} \left\{ \frac{e^{st}}{F(s)} \right\}_{s = \alpha_k} = \frac{e^{\alpha_k t}}{F'(\alpha_k)}.$$

Hence, the impulse response is

$$g(t) = K \sum_{k=1}^{\infty} \frac{e^{\alpha_k t}}{F'(\alpha_k)}, \tag{12}$$

which is exactly the pulse response of the rational transfer function

$$H(s) = \sum_{k=1}^{\infty} \frac{K}{F'(\alpha_k)(s-\alpha_k)}. \tag{13}$$

Since this transfer function must have the same stationary gain as $G(s)$, that is, $G(0)$, the Final Value Theorem implies that the sum in Eq. 13 is convergent for $s = 0$ (Levine, 1996). Further, the singularities α_k become largely negative with increasing k, which means that the terms represent faster and faster dynamic modes. Hence, only the first terms in the sum are significant for describing the dynamics. An arbitrarily good approximation can, therefore, be achieved by truncating the sum after m terms. Adding the stationary gain of the ignored terms to achieve a correct description of the steady-state behavior then gives

$$\hat{G}(s) = \sum_{k=1}^{m} \frac{K}{F'(\alpha_k)(s-\alpha_k)} + G(0) + \sum_{k=1}^{m} \frac{K}{F'(\alpha_k)\alpha_k}. \tag{14}$$

If the transfer function is required to be strictly proper (Levine, 1996), the addition of the ignored gain can be omitted. If it is required to be strictly proper *and* have correct stationary gain, the sum of transfer functions may instead be multiplied by

$$-G(0)\left(\sum_{k=1}^{m} \frac{K}{F'(\alpha_k)\alpha_k}\right)^{-1}.$$

Several other, and well-established methods, which are based on approximations of the biofilm mass balances (Eqs. 2 and 3), can be used to derive rational transfer functions for the CSBR model. These methods keep the bulk mass balance (Eq. 1) as it is and, thus, one state variable is always used for the bulk concentration. In the proposed "residue method" the approximations are made in the frequency plane, instead of in space, and, therefore, it is the combined behavior of both mass balances that is approximated. For low-order approximations, the residue method can therefore be expected to give better accuracy, particularly up to frequencies around α_{m+1}.

In Figure 2 the performance of the residue method is compared to two common methods: a finite difference method and the Galerkin MWR-method using Legendre polynomials. The former one is intuitive and simple to formulate, and the Galerkin method generally gives very accurate low-order approximations (Finlayson, 1972). The application of these methods to the CSBR problem is described in the Appendix. It should be noted that for this particular problem the Galerkin method equals that of the least-squares method, which minimizes the integral of the squared error of Eq. 2 when c is replaced by its approximation $\hat{c}$.

A few general features of the different approximation methods are apparent in Figure 2. The residue method gives incorrect high frequency gains due to the direct terms in Eq. 14, while the finite difference method and the Galerkin method have errors in the stationary gains. This stationary

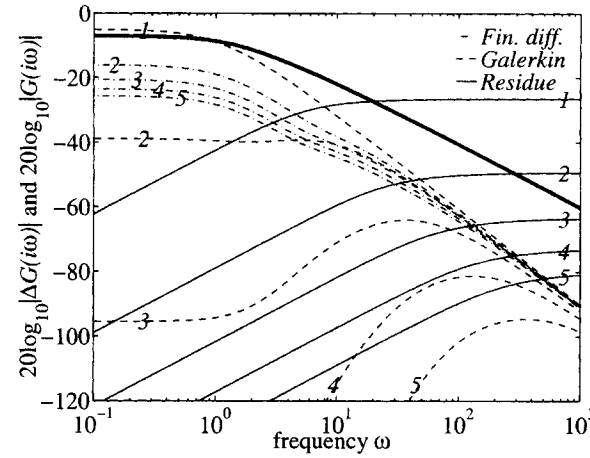

Figure 2. Amplitude of $G(i\omega)$ (thick line) for planar substrata with $\tau = 1$, $\gamma = 1$ and $\kappa = 2$ and amplitudes of the approximation errors $\Delta G(i\omega) = G(i\omega) - \mathbf{G}(i\omega)$ for transfer function orders up to $m = 5$.

The lowest order of the finite difference method is $m = 2$.

bias is zero when $\kappa = 0$ but increases as κ increases. For higher-order approximations ($m > 4$), the Galerkin method gives the best approximations. However, for the frequencies of particular interest in controller design, that is, where the gain of G starts to decrease, the low-order approximations ($m < 4$) of the residue method are the most accurate. Already, a first-order transfer function may give accurate results if κ is large. This is particularly advantageous when several CSBRs are used to model a reactor since it may then be crucial to keep the order of the approximations at a minimum. As can be expected, the finite difference method gives the least accurate approximations.

Application to Trickling Filters

To illustrate the use of the transfer functions, the model approach is applied to a nitrifying trickling filter (NTF) that oxidizes ammonium in tertiary wastewater into nitrate. The large pilot-scale plant, described by Wik (1997), is 7.2 m high, 2.7 m in diameter, and filled with a cross-flow plastic media with a surface that can be assumed planar. Prior to the experiments presented here, the plant had been operating for several years and the entire media, having a total area of $A_r = 9{,}320$ m^2, can be assumed to have been covered with a well-established biofilm.

Due to the mixing in the bulk experienced in trickling filters they have been modeled as cascaded CSBRs by Rittmann (1982), Wanner and Gujer (1984), Gujer and Boller (1986), Wik and Lindeborg (1994), Wik et al. (1995), Wik (1997), Vayenas and Lyberatos (1994), and Vayenas et al. (1997). Here, the plant is modeled as n identical CSBRs with a planar biofilm substratum. The parameter values used in the modeling are presented in Table 1. The diffusion coefficients are set to 80% of the values in water, and the value of the biofilm porosity is a value for well-established nitrifying biofilms that has been used in previous investigations of the

Table 1. Model Parameters as Functions of Water Temperature T (°C)

D_{NH_4}	$(730+12.8T+0.606T^2-0.00533T^3)\times 10^{-7}$	m^2/d	Gujer and Boller (1986)
D_{Li}	$(400+14.9T+0.143T^2)\times 10^{-7}$	m^2/d	Lobo and Quaresma (1989)
ϵ	0.3	$m^3\cdot m^{-3}$	Wik et al. (1995)
V	V_r/n	m^3	This work
A	9,320/n	m^2	Plant spec.
L	0.0003 – 0.0015	m	This work
D_{O_2}	$(682+29.8T-0.0343T^2+0.016T^3)\times 10^{-7}$	m^2/d	Gujer and Boller (1986)
$c_{O_2}^{sat}$	$14.53-0.411T+9.6\times 10^{-3}T^2-1.2\times 10^{-4}T^3$	g O_2/m^3	Riley and Skirrow (1975)

plant by Wik and Lindeborg (1994), Wik et al. (1995), and Wik (1997).

Wik et al. (1995) have carried out five pulse response experiments on the plant at the water temperature 10.1°C, with dissolved LiCl as trace substance, at the two different flows $Q = 14.5$ L/s and $Q = 7.3$ L/s. Since LiCl is not involved in any reaction, the response will be that of a zero-order reaction, that is, $\kappa = 0$.

Assigning values of the remaining unknown parameters n, L and the total bulk water volume V_r in the NTF, the first principle and the approximate transfer function for the NTF in the original time scale can be determined from

$$G(s) = \frac{1}{\left(1+\tau s/\lambda+\gamma\sqrt{s/\lambda}\tanh\sqrt{s/\lambda}\right)^n} \tag{15}$$

$$\hat{G}(s) = \left[\sum_{k=1}^{m}\frac{1}{F'(\alpha_k)(s/\lambda-\alpha_k)}+G(0)+\sum_{k=1}^{m}\frac{1}{F'(\alpha_k)\alpha_k}\right]^n, \tag{16}$$

where $\lambda = D/(L^2\epsilon)$ is the time-scaling factor.

After determination of the solutions y_k to Eq. 7 with a Newton-Raphson search on the intervals (Eq. 8), the singularities $\alpha_k = -y_k^2$, the derivatives $F'(\alpha_k) = \tau + (\gamma/2y_k)(y_k + \tan y_k + y_k\tan^2 y_k)$, and $\hat{G}(s)$ can be determined. Pulse responses may then efficiently be simulated with standard routines in the software MATLAB, which allows for estimation of reactor parameter by means of least-squares fitting to experimental data.

For the pulse response experiments, all carried out on the same day, the biofilm thickness can be assumed to be the same at both flows. The number of CSBRs, n, is also set to be the same, while the bulk volume V_r, which, unfortunately, was not possible to measure, most likely depends on the flow. Hence, the unknown parameters to be estimated from the experiments are n, L and the bulk volume V_r at the two different flows.

The best fit was achieved, successively for increasing n, by applying the nonlinear least-squares algorithm by Levenberg and Marquardt in MATLAB Optimization Toolbox (MathWorks, 1996) to minimize the sum of the squared differences $e(t_i)$ between the measured effluent lithium concentrations and the responses of $\hat{G}$.

There are two simple methods to speed up the identification process. One is to use only a few singularities at the beginning, such as $m = 2$ or $m = 3$, and then increase m to improve the accuracy. The other one is to calculate good initial values for the least-squares algorithm. This can be achieved by using the mean residence time and the variance of the measured residence time distributions. From the transfer function (Eq. 15) the mean residence time can be determined as

$$T = \frac{\int_0^\infty t c_{out}(t)dt}{\int_0^\infty c_{out}(t)dt} = -\lim_{s\to 0}\frac{d}{ds}G(s) = \frac{V_r + A_r\epsilon L}{Q} \tag{17}$$

and the variance as

$$\sigma^2 = \frac{\int_0^\infty (t-T)^2 c_{out}(t)dt}{\int_0^\infty c_{out}(t)dt} = \lim_{s\to 0}\frac{d^2}{ds^2}G(s) - T^2 = \frac{2A_rL^3\epsilon^2}{3QD}+\frac{T^2}{n}. \tag{18}$$

Insertion of n into the expression for σ^2 gives initial values for L, which, after insertion into the expression for T, gives initial values for V_r.

The best fit, shown in Figures 3 and 4, was found for $n = 10$ and the parameter values $\theta = [V_{r1}\ V_{r2}\ L]^T = [2.40\ m^3\ 3.20\ m^3\ 0.64\ mm]^T$. Calculating the differences $e(t_k)$

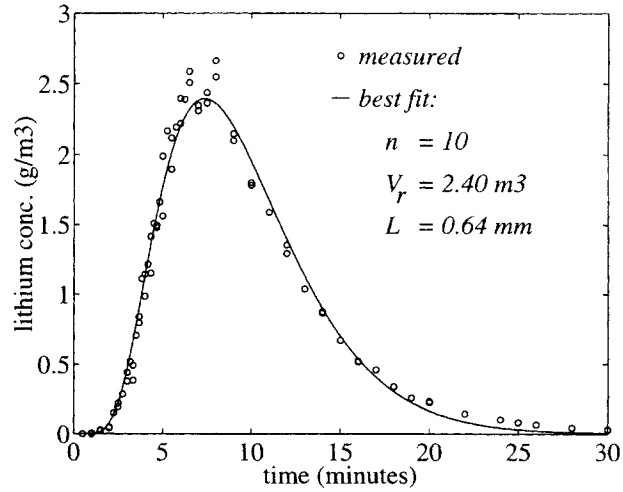

Figure 3. Pulse responses at Q = 7.3 L/s.

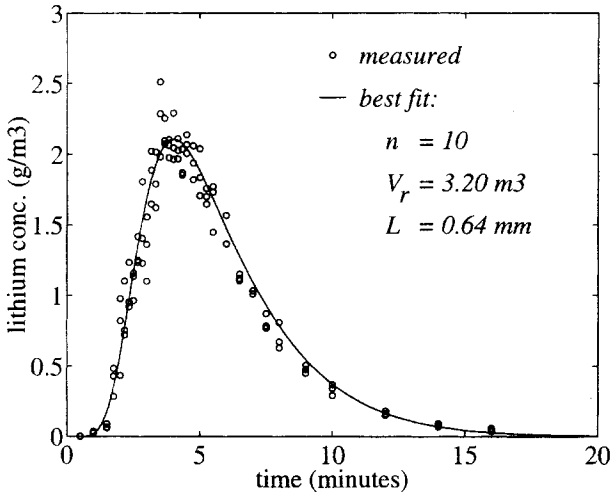

Figure 4. Pulse responses at $Q = 14.5$ L/s.

and the Jacobian $(de/d\theta)$ for these values of n and θ, the covariance matrix for the identified parameters can be estimated as (Ljung, 1987, p. 243)

$$\mathrm{Cov}(\hat{\theta}) = \frac{1}{N}\sum_{t_k} e^2(t_k)\left[\sum_{t_i}\left(\frac{de(t_i)}{d\theta}\right)\left(\frac{de(t_i)}{d\theta}\right)^T\right]^{-1}$$

$$= 10^{-3}\begin{bmatrix} 0.556 & 0.025 & -0.122 \\ 0.025 & 0.508 & -0.026 \\ -0.122 & -0.026 & 0.127 \end{bmatrix},$$

where $N = 175$ is the number of measurements. The small variance shows that the dependencies of the estimated values on each other are weak.

When $n = 10$, Eqs. 17 and 18 and the measured mean residence times and variances give $L = 0.80$ mm and $V_{r1} = 2.20$ m^3 for $Q = 7.3$ L/s. $L = 0.63$ mm and $V_{r2} = 3.1$ m^3 for $Q = 14.5$ L/s, which are fairly close to the values estimated with the least-squares method.

Using the parameter values estimated from the pulse responses, the dynamics caused by changes in influent ammonium load can be modeled. Two step response experiments, where the influent ammonium concentration was raised from a very low level to a high level, have been carried out on the plant. Wik (1997) found a close agreement between experimental data and simulated data with a nonlinear model identical to the one used for the pulse responses except that the reaction rate was modeled by a Monod expression.

At high ammonium concentrations, oxygen, which is dissolved in the bulk from the air, is the rate limiting substrate and the nitrification rate can be assumed independent of the ammonium concentration (Gönenç and Harremoës, 1985). Hence, the dynamics will be that of a zero-order reaction and the only difference from the model used to describe the pulse response experiments is the value of the diffusion coefficient. After linear interpolation of the bulk volume as a function of the flow and insertion of the diffusion coefficient for ammonium, the approximate transfer function (Eq. 16) at the operating point $Q = 12.3$ L/s can be determined. If the transfer function is going to be used for controller design, used in model-based controllers, or for real-time simulations where the NTF is only a subprocess, it is desirable to keep the transfer function as low order as possible, that is, as few terms as possible in the sum of Eq. 16 should be used.

Table 2. Singularities and Derivatives

k	1	2	3	4	5	6
y_k	1.30	2.42	4.87	7.94	11.1	14.2
α_k	−1.70	−5.87	−23.7	−63.0	−122	−201
$F'(\alpha_k)$	1.35	0.31	2.96	9.90	20.5	34.7
$-1/[F'(\alpha_k)\alpha_k]$	0.435	0.548	0.014	0.002	0.000	0.000

The larger the solutions y_k are on the imaginary axis, the larger the derivatives $F'(\alpha)$ are, since the solutions are located closer and closer to the singularities of tan y. Since the poles α_k also become larger and larger, the contribution $-1/[F'(\alpha_k)\alpha_k]$, that each term in the sum of $\hat{G}(s)$ contributes to the total gain, becomes less and less significant. In Table 2 the relevant values in the determination of $\hat{G}(s)$ are listed for the first six singularities.

From the values of α, we see that, already, the third dynamic mode is about 14 times faster than the slowest mode, and the fourth dynamic mode is more than 37 times faster. The values of $-1/[F'(\alpha_k)\alpha_k]$ show that the two first terms terms in Eq. 14 contribute to 98.3% of the stationary gain of one CSBR and the three first terms contribute to 99.8%. After noting this, it can be concluded that the sum in Eq. 16 should be truncated after two or three terms if a low-order model is required. The third mode can only affect the dynamics significantly when changes in the influent concentration have frequencies in the order of $-\lambda\alpha_3 = 12.9$ rad/min, or faster. This is faster than can be expected under normal operation of the plant and, hence, a truncation after two terms should be enough. Equation 16 then gives the following transfer function in a minute time scale

$$\hat{G}(s) = \left(\frac{0.435}{1+1.0796s} + \frac{0.548}{1+0.3124s} + 0.016\right)^{10}. \quad (19)$$

In Figure 5 the Bode plots of this transfer function are compared to those of the first principle transfer function (Eq. 15). As can be seen from the figure, the curves of the first principle transfer function and those of the rational approximation almost coincide in the frequency region considered. The disagreement is in the high frequency region as a consequence of the ignored fast dynamic modes. However, the disagreement is not of any practical importance, not only because such fast changes do not occur under normal operation, but also since there is almost no effect of changes in influent concentration on the effluent concentration, then, due to the low values of the gain $|G(i\omega)|$ at high frequencies.

Unfortunately, no experimental data that can be used for validation of this zero-order reaction model were collected from the pilot plant before it was taken out of operation in 1996. However, fast sampled data from an experiment, where

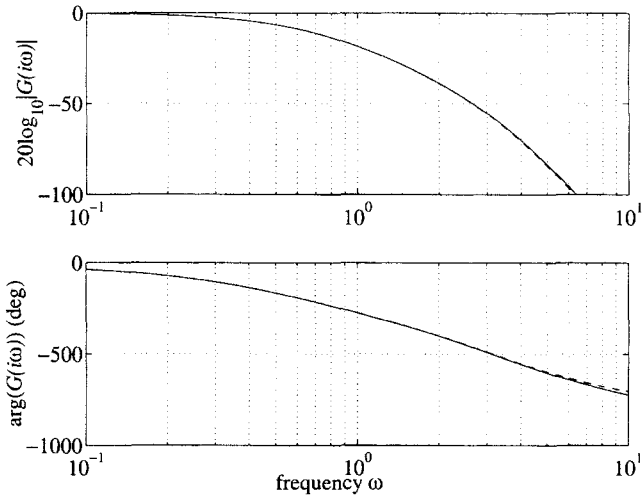

Figure 5. Bode diagram of $G(i\omega)$ (solid) and $G(i\omega)$ (dashed) for the NTF model.

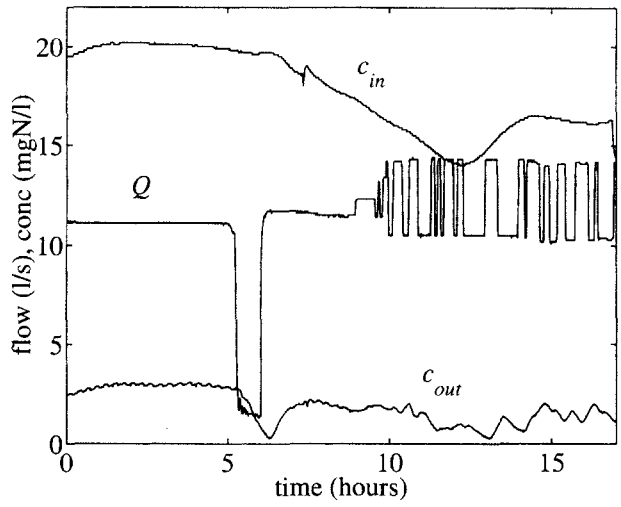

Figure 6. Measured flow, influent ammonium concentration, and effluent ammonium concentrations vs. time.

the flow through the plant was rapidly changed around an operating point, are available. The operating point at that time was only partly in the region where the nitrification rate can be assumed to have been of zero order. In the upper parts of the plant, the ammonium concentration was high enough for oxygen to be rate limiting and for the zero-order assumption to hold. However, in the lowest parts the concentration was low enough for ammonium to affect the reaction rate.

Assuming that the bulk is saturated with oxygen, the transition level for the ammonium bulk concentration between oxygen limitation and ammonium limitation can be estimated by (Szwerinski et al., 1986; Gujer and Boller, 1986)

$$c_{\mathrm{NH_4}}^{\lim} = \frac{D_{\mathrm{O_2}}}{4.33 D_{\mathrm{NH_4}}} c_{\mathrm{O_2}}^{\mathrm{sat}},$$

which is 2.7 mg N-NH_4^+/L for the average water temperature $T = 12.2$°C during the experiment.

The influent concentration varied from 15 to 20 mg N-NH_4^+/L and the effluent concentration was around 2 mg N-NH_4^+/L (see Figure 6). Hence, at the very lowest parts of the plant, the nitrification rate depends on the ammonium concentration.

For varying flow, the mass-balance (Eq. 1) results in a nonlinear model. However, since the flow was varied around an operating point $Q_0 = 12.3$ L/s, a linearized mass balance can be used. If an equivalent influent ammonium concentration

$$\tilde{c}_{\mathrm{in}}(t) = \frac{Q(t) c_{\mathrm{in}}(t)}{Q_0},$$

is used as input to the model, the transfer function of the linearized model equals (Eq. 19) if the reaction is of zero order in the entire NTF. Due to the low effluent concentration, however, the reaction in the last CSBR is assumed to be of first order with $\kappa = 130$. For this value, already, the second mode is 12 times faster than the slowest mode and nearly 80 times faster than the slowest mode of the zero-order CSBRs. Hence, the sum in Eq. 14 may be truncated after only one term, which also contributes to more than 99.9% of the total gain $1/(1+\gamma\sqrt{\kappa}\tanh\sqrt{\kappa})$ of the last CSBR. Combining the resulting transfer function with those of the nine zero-order CSBRs gives the following transfer function of the NTF-model

$$\hat{G}(s) = \left(\frac{0.435}{1+1.0796s} + \frac{0.548}{1+0.3124s} + 0.016\right)^9 \times \left(\frac{0.399}{1+0.164s} + 6.1\cdot 10^{-4}\right).$$

The dynamics in the last CSBR is faster than in the others, and the influent concentrations also vary slower than in the upper parts of the NTF. Thus, the transfer function for the last CSBR may actually be reduced to only the constant gain 0.4.

The effluent ammonium concentration was measured by a continuous ammonium meter of a titration kind, which has been modeled and validated by Wik (1997). In Figure 7, where simulated and measured data are shown, the simulated measured ammonium concentration is the output of that model when the simulated effluent of the NTF is used as meter model input. As can be seen from the figure, the simulated dynamics agree with the measurements except during a period after 6 h, where the flow suddenly dropped far below the operating point.

Conclusion and Discussion

Using standard assumptions for the biofilm, nonrational transfer functions have been derived describing the fast dynamic modes of continuously-stirred biofilm reactors (CSBRs) when the intrinsic reaction rate is of zero or first order and the biofilm substrata are planar, cylindrical, or spherical in

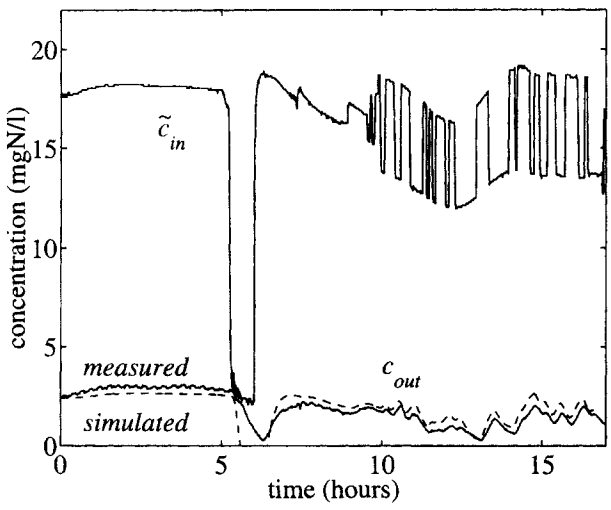

Figure 7. Ammonium concentrations: equivalent influent, measured effluent (solid) and simulated effluent (dashed).

shape. The same equations and transfer functions may also be applied to catalytic reactors with porous catalysts. A method, based on the fact that the singularities of the transfer functions are spread out along the negative real axis, has been introduced to derive rational transfer functions that approximate the nonrational ones. These approximations have several appealing properties:

- Efficient routines for simulations, using the rational transfer function models, are available in most types of numerical software.
- Many standard methods of controller design require rational transfer functions.
- The derivation only requires Newton-Raphson searches for the values of the singularities and evaluation of a few expressions.
- Changes in physical parameters, in particular, the first-order rate coefficient that may depend significantly on temperature, can easily be related to changes in the transfer function.
- Since the approximation is based on truncation of a sum of first-order transfer functions with decreasing time constants and decreasing gain, the order of the approximate transfer function can be chosen for a specific application in a natural way and without any recalculations.

The methods have successfully been applied to a model of a nitrifying trickling filter, where the reactor was modeled by n cascaded CSBRs. The approximate transfer function and the first principle transfer function were used to estimate reactor and biofilm parameters from residence-time distributions. Using the estimated values, transfer functions describing the dynamics caused by changes in influent ammonium concentration and influent flow were derived. Based on the values of the singularities, it was possible to use only second-order transfer functions for each CSBR, that is, the n mass balances over the CSBRs and the n second-order partial differential equations describing the concentrations in the biofilm could be replaced by n second-order ordinary differential equations.

Although the work presented only considers the concentration of one substrate and single-input, single-output (SISO) transfer functions, the methods may also be applicable to systems where more than one concentration is considered and to the corresponding multi-input, multi-output (MIMO) transfer functions.

Acknowledgments

We would like to thank our colleague Prof. Bengt Andersson at the Dept. of Chemical Reaction Engineering for valuable discussions on the topic of catalytic reactors, and the School of Environmental Sciences, Göteborg University/Chalmers University of Technology that, to a large extent, financed this work.

Literature Cited

Andersson, B., H. Aspegren, D. S. Parker, and M. P. Lutz, "High Rate Nitrifying Trickling Filters," *Wat. Sci. Tech.*, **29**, 47 (1994).

Aris, R., *The Mathematical Theory of Diffusion and Reaction in Permeable Catalysts*, Vol. 1, Clarendon Press, Oxford (1975).

Atkinson, B., and I. S. Daoud, "The Analogy between Micro-Biological 'Reactions' and Heterogeneous Catalysis," *Trans. Instn. Chem. Engrs.*, **46**, T19 (1968).

Boller, M., M. Tschui, and W. Gujer, "Effects on Transient Nutrient Concentrations in Tertiary Biofilm Reactors," *Wat. Sci. Tech.*, **36**, 101 (1997).

Finlayson, B. A., *The Method of Weighted Residuals and Variational Principles*, Academic Press, New York (1972).

Fischer, S. D., *Complex Variables*, Mathematics series, 2nd ed., Wadsworth and Brooks/Cole, Pacific Grove, CA (1990).

Gönenç, I. E., and P. Harremoës, "Nitrification in Rotating Disc Systems: I," *Wat. Res.*, **19**, 1119 (1985).

Gujer, W., and M. Boller, "Design of a Nitrifying Tertiary Trickling Filter Based on Theoretical Concepts," *Wat. Res.*, **20**, 1353 (1986).

Gujer, W., and O. Wanner, "Modelling Mixed Population Biofilms," *Biofilms*, W. G. Characklis and K. C. Marshall, eds., Wiley, New York (1990).

Kissel, J. C., P. L. McCarty, and R. L. Street, "Numerical Simulation of Mixed Culture Biofilm," *J. Environ. Eng.*, **110**, 393 (1984).

Levine, W. S., *The Control Handbook*, Chap. 2, CRC Press, Boca Raton, FL (1996).

Ljung, L., *System Identification—Theory for the User*, Prentice Hall, Englewood Cliffs, NJ (1987).

Lobo, V. M. M., and J. L. Quaresma, *Handbook of Electrolyte Solutions: Part B*, Physical Science Data 41, Elsevier, Amsterdam (1989).

MathWorks, *MATLAB Optimization Toolbox, User's Guide*, 2nd ed., The MathWorks Inc., Natick, MA (1996).

Råde, L., and B. Westergren, *BETA—Mathematics Handbook*, 2nd ed., Studentlitteratur and Chartwell-Bratt, Lund, Sweden (1990).

Riley, J. P., and G. Skirrow, *Chemical Oceanography*, Vol. 4, 2nd ed., Academic Press, London (1975).

Rittmann, B. E., "Comparative Performance of Biofilm Reactor Types," *Biotechnol. Bioeng.*, **24**, 1341 (1982).

Rittmann, B. E., "The Effect of Load Fluctuations on the Effluent Concentration Produced by Fixed-Film Reactors," *Wat. Sci. Tech.*, **17**, 45 (1985).

Szwerinski, H., E. Arvin, and P. Harremoës, "pH-Decrease in Nitrifying Biofilms," *Wat. Res.*, **20**, 971 (1986).

Vayenas, D. V., and G. Lyberatos, "A Novel Model for Nitrifying Trickling Filters," *Wat. Res.*, **28**, 1275 (1994).

Vayenas, D. V., S. Pavlou, and G. Lyberatos, "Development of a Dynamic Model Describing Nitrification and Nitratification in Trickling Filters," *Wat. Res.*, **31**, 1135 (1997).

Wanner, O., and W. Gujer, "Competition in Biofilms," *Wat. Sci. Tech.*, **17**, 27 (1984).

Wik, T., "Modelling Dynamics of Nitrifying Trickling Filters and Ammonium Meters," *Med. Fac. Landbouww. Univ. Gent*, **62**, 1641 (1997).

Wik, T., and C. Lindeborg, "Modelling the Dynamics of a Trickling Filter for Waste Water Treatment," *Proc. 3rd IEEE Conf. on Control Appl.*, Glasgow, U.K., p. 1035 (1994).
Wik, T., A. Mattsson, E. Hansson, and C. Niklasson, "Nitrification in a Tertiary Trickling Filter at High Hydraulic Loads," *Wat. Sci. Tech.*, **32**, 185 (1995).
Wik, T., and C. Breitholtz, "Steady-State Solution of a Two-Species Biofilm Problem," *Biotech. Bioeng.*, **50**, 675 (1996).

Appendix

Sign of Im $\{M(z)\}$

Planes. If we write the complex variable z as $x+iy$ and use the fact that (Råde and Westergren, 1990)

$$\tanh z = \frac{\sinh 2x}{\cosh 2x+\cos 2y} + i\frac{\sin 2y}{\cosh 2x+\cos 2y},$$

the imaginary part of $M(z)$ becomes

$$\mathrm{Im}\{M(z)\} = \frac{x\sin 2y + y\sinh 2x}{\cosh 2x+\cos 2y},$$

which has the same sign as xy.

On the real axis we have $M(x)=x\tanh x$, which is a positive even function in x.

Cylinders. To show that the imaginary part of $M(z)$ has the same sign as xy for cylinders is not as straightforward as for planes and spheres. From physical insight, we know that $M(z)$ approaches $M(z)$ for planes as ρ approaches one and, hence, the sign of Im$\{M(z)\}$ must, in this case, equal that of xy. Using, for example, the fact that both $I_0(z)$ and $zI_1(z)$ are infinite sums of z^2, it is readily shown that the imaginary part of $M(z)$ is an odd function in both x and y and, hence, the sign of Im$\{M(z)\}$ equals that of xy for all x and y if the first quadrant is mapped onto the upper half-plane. With this background and from numerous numerical calculations, we conclude that so is the case for all values of ρ.

On the real axis we have

$$M(x) = x\frac{K_1(\rho x)I_1(x) - K_1(x)I_1(\rho x)}{K_1(\rho x)I_0(x) + K_0(x)I_1(\rho x)}.$$

The modified Bessel functions I_0 and K_0 are positive even functions in x, while I_1 and K_1 are odd functions with the same sign as their arguments. Further, since $\rho<1$, we have $I_1(x)>I_1(\rho x)$ and $K_1(\rho x)>K_1(x)$. Hence, $M(x)$ is a positive even function in x.

Spheres. Setting $\delta z = x+iy$ gives (Råde and Westergren, 1990)

$$\cosh \delta z = \cosh x\cos y + i\sinh x\sin y$$

$$\sinh \delta z = \sinh x\cos y + i\cosh x\sin y.$$

Denoting the denominator of the quotient in $M(z)$ by $D(z)$, it is straightforward to show, using these expressions and rules for trigonometric and hyperbolic functions, that

$$|D|^2\mathrm{Im}\{M(z)\} = Im_1 + (\rho/\delta)^2(x^2+y^2)Im_3 + (\rho/\delta)xyIm_3,$$

where

$$Im_1 = \frac{1}{2}(y\sinh 2x - x\sin 2y)$$

$$Im_2 = \frac{1}{2}(y\sinh 2x + x\sin 2y)$$

$$Im_3 = 2(1+\sinh^2 x - \cos^2 y).$$

Im_1 and Im_2 have the same sign as xy, $Im_3 \geq 0$, and $D(z)$ has no singularities in any of the quadrants. Hence, also Im$\{M(z)\}$ has the same sign as xy.

On the real axis, $M(z)$ can be written as

$$M(x) = \frac{\delta x - \tanh \delta x + \rho x^2\tanh \delta x}{\rho x + \tanh \delta x},$$

which is a quotient of odd functions and, thus, is a positive even function in x.

Approximation methods in the comparison

Residue Method. Since $\kappa > 1/\tau$, there is one singularity corresponding to a solution to Eq. 6 on the real axis. Hence, solve Eq. 6 with $z=x>0$ to get the singularity $\alpha_1 = x^2-\kappa$. The remaining singularities $\alpha_k = y_k^2-\kappa$, $k=2\ldots m$ follow from solving Eq. 7 on the intervals $[\pi(k-1/2), \pi(k+1/2)]$. Then calculate

$$F'(\alpha_1) = \tilde{\tau} + \frac{\tilde{\gamma}}{2x}(x+\tanh x - x\tanh^2 x)$$

$$F'(\alpha_k) = \tilde{\tau} + \frac{\tilde{\gamma}}{2y_k}(y_k + \tan y_k + y_k\tan^2 y_k), \quad k=2\ldots m$$

$$G(0) = 1/(1+\gamma\sqrt{\kappa}\tanh\sqrt{\kappa}),$$

and insert these values and the values of α_k in Eq. 14, which gives a mth-order transfer function.

Finite Difference Method. Let $\xi_k = k\xi/m$, $k=0,1,\ldots m$ be a discretization of the biofilm. Use symmetric central differences to approximate the second-order space derivative in Eq. 2 and define an approximation $c_k(t)$ of $c(\xi_k,t)$ by

$$\frac{dc_k}{dt} = \frac{c_{k-1}-2c_k+c_{k+1}}{(1/m)^2} - \kappa c_k, \quad k=1,2,\ldots m-1,$$

$$c_1 = c_0 \quad \text{and} \quad c_m = c^b,$$

where the bulk concentration is approximated by

$$\tau\frac{dc^b}{dt} = c_{\mathrm{in}}^b - c^b - \gamma\frac{c_m - c_{m-1}}{(1/m)}.$$

The above equations can be written in the state-space form $\dot{x} = Ax + Bc_{\mathrm{in}}^b$, $c^b = Cx$, where $x=[c_1\ldots c_m]$, A is a tridiagonal matrix, $B=[0\ldots 0\ 1/\tau]$, and $C=[0\ldots 0\ 1]$. A mth-order transfer function is then given by $\hat{G}(s) = C[sI-A]^{-1}B$.

Galerkin Method Using Legendre Polynomials. Extend the mass balance (Eq. 2) to $-1 < \xi < 1$. Since the solution must be symmetric around $\xi = 0$, we approximate the concentration in the biofilm with the trial function

$$\hat{c}(t, \xi) = \sum_{k=0}^{m-1} x_k(t) P_{2k}(\xi),$$

where P_{2k} are Legendre polynomials of order $2k$, orthogonal on $(-1, 1)$ and normed such that $P_{2k}(1) = 1$. Forcing this approximation to satisfy the boundary condition $\hat{c}(1, t) = c^b$, setting the weighted residuals to zero and inserting the approximation into Eq. 1 give

$$\sum_{k=0}^{m-1} x_k = c^b$$

$$0 = \sum_{k=0}^{m-1} \left\{ \dot{x}_k(P_{2n}, P_{2k}) - x_k \left[\left(P_{2n}, \frac{d^2 P_{2k}}{d\xi^2} \right) - \kappa(P_{2n}, P_{2k}) \right] \right\}$$

$$n = 0, 1, \ldots m-1$$

$$\tau \dot{c}^b = c^b_{\text{in}} - c^b - \gamma \sum_{k=0}^{m-1} x_k \left. \frac{dP}{d\xi} \right|_{\xi=1}$$

where $(u, v) = \int_{-1}^{1} uv d\xi$. Use the first equation to eliminate, for example, x_{m-1} in the other two equations. The result may then be written in linear state space form from which a mth-order transfer function $\hat{G}(s)$ can be derived in the same manner as with the finite difference method.

Manuscript received Mar. 6, 1998, and revision received Sept. 10, 1998.